Electronic Supplementary Material (ESI) for Journal of Materials Chemistry A.

Supplementary materials:

From nanomelting to nanobeads: Nanostructured Sb_xBi_{1-x} alloys anchored in three-dimensional carbon frameworks as a high-performance anode for potassium-ion batteries

Xiao-Dong He, [a] Jia-Ying Liao, [a] Shuo Wang, [a] Jun-Ru Wang, [a] Ze-Hua Liu, [a] Xiang Ding, [a] Qiao Hu, [a] Zhao-Yin Wen, [b] Chun-Hua Chen *[a]

[a]*CAS Key Laboratory of Materials for Energy Conversions, Department of Materials Science and Engineering & Collaborative Innovation Center of Suzhou Nano Science and Technology, University of Science and Technology of China, Anhui Hefei 230026, China*

[b]*Key Laboratory of Energy Conversion Laboratory, Shanghai Institute of Ceramics, Chinese Academy of Sciences, Shanghai 200050, China*

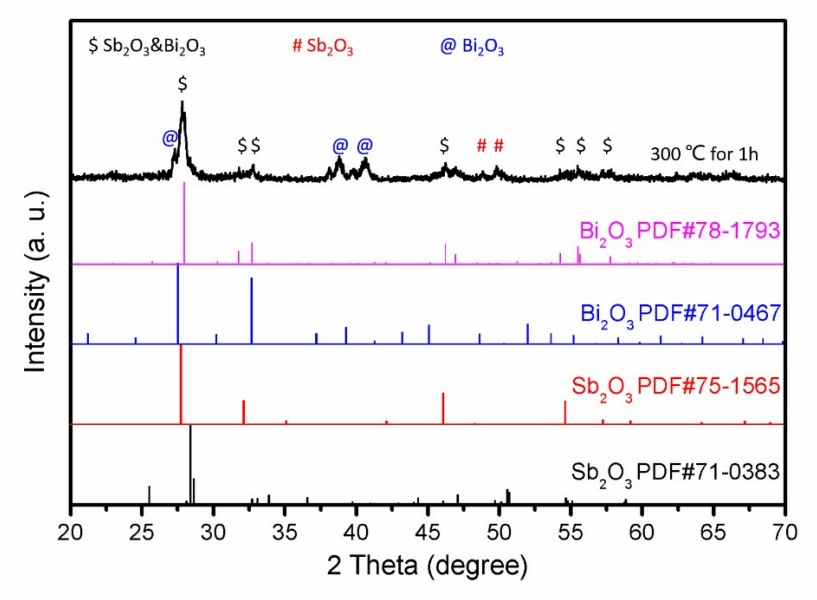

Fig. S1 XRD pattern of the polymeric precursor resin after sintering at 300 °C for 1h.

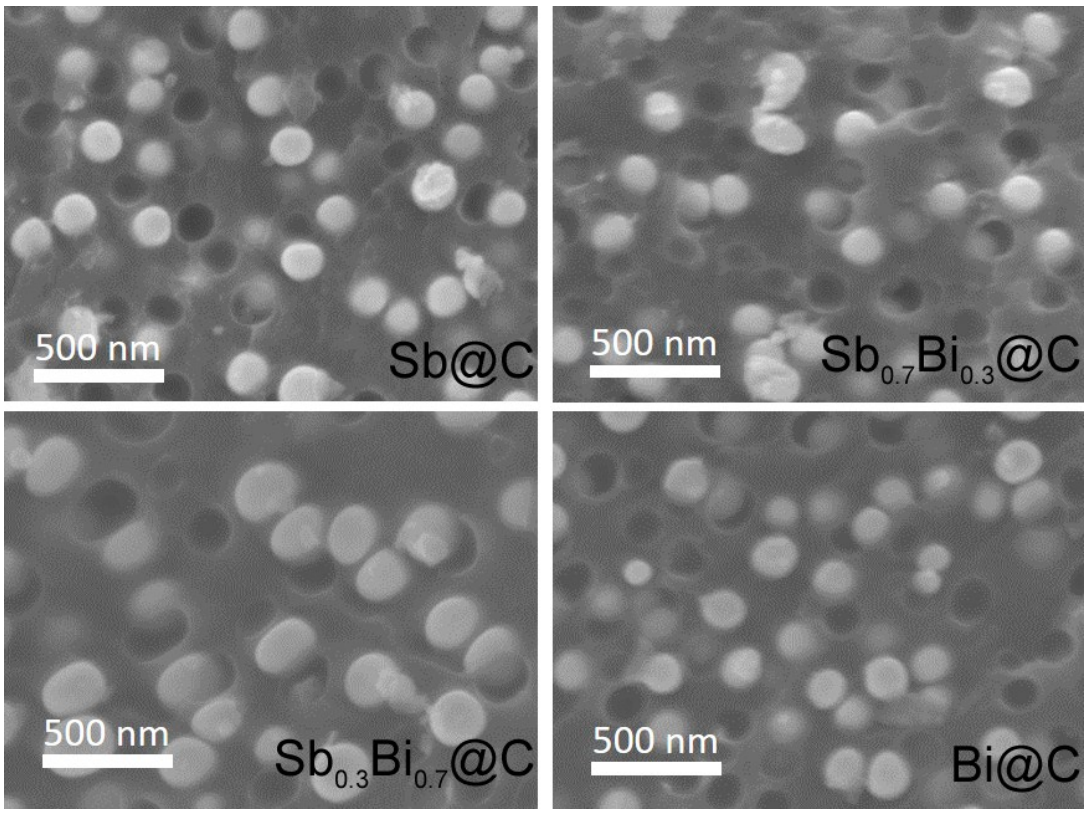

Fig. S2 FESEM images of (a) Sb@C, (b) $Sb_{0.7}Bi_{0.3}$@C, (c) $Sb_{0.3}Bi_{0.7}$@C and (d) Bi@C.

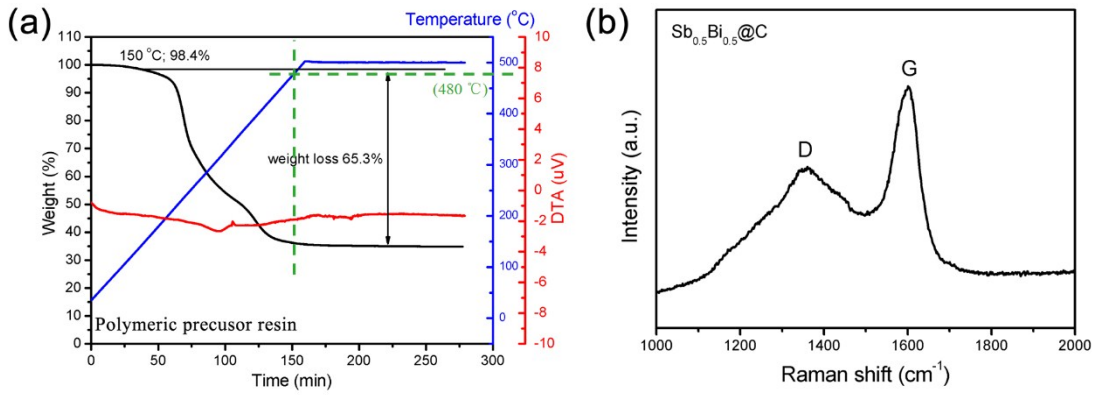

Fig. S3 (a) TGA-DTA curves of the polymeric precursor resin. (b) Raman spectra of the $Sb_{0.5}Bi_{0.5}$@C composite.

From the TGA-DTA curves (Fig. S3a), the weight of the polymeric precursor resin keeps constant after about 480°C, which indicates the complete carbonization of the polymeric precursor resin at about 480°C. The treatment temperature at 500°C is thus sufficient to have complete carbonization. Furthermore, the Raman spectra of the $Sb_{0.5}Bi_{0.5}$@C composite (Fig. S3b) can also confirm the formation of carbon in the nanocomposites. In addition, our newly-added XPS analysis also confirms the formation of carbon (see below in Fig. S4c).

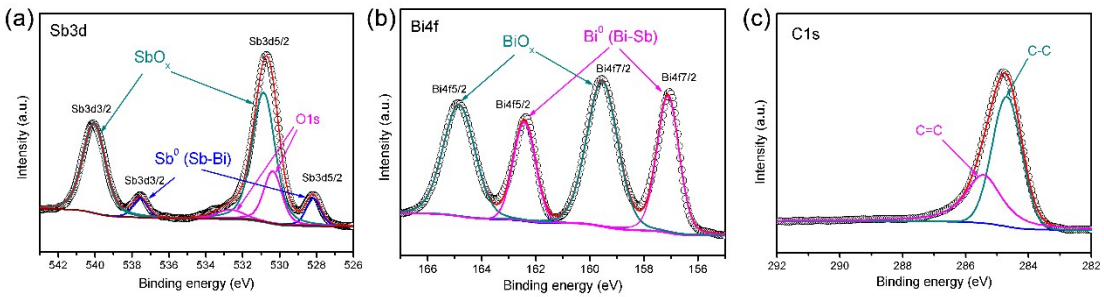

Fig. S4 XPS spectra of the $Sb_{0.5}Bi_{0.5}$@C composite. (a) Sb 3d. (b) Bi 4f. (c) C 1s.

The XPS spectra of the $Sb_{0.5}Bi_{0.5}$@C composite are illustrated in Fig. S4. Nevertheless, as reported in literature (e.g. Nano Energy 2019, 66, 104133 for Sb, e.g. Adv. Energy Mater. 2018, 8, 1703288 for Bi), the easy surface oxidation of the alloy components Sb and Bi is difficult to be avoided and therefore detected by XPS. Specifically, two peaks located at 540.07 and 530.88 eV are attributed to Sb 3d3/2 and 3d5/2 from SbO_x (Fig. S4a), respectively. The Sb^0 in $Sb_{0.5}Bi_{0.5}$ alloy is proved by the peaks at 537.54 and

528.18 eV. Two peaks located at 164.85 and 159.53 eV in the Bi 4f spectrum are assigned to BiO_x (Fig. S4b). The Bi^0 in $Sb_{0.5}Bi_{0.5}$ alloy is confirmed by the peaks at 162.43 and 157.11 eV. These higher oxidation peak are derived from the surface oxidation of the $Sb_{0.5}Bi_{0.5}$ alloy in the air.

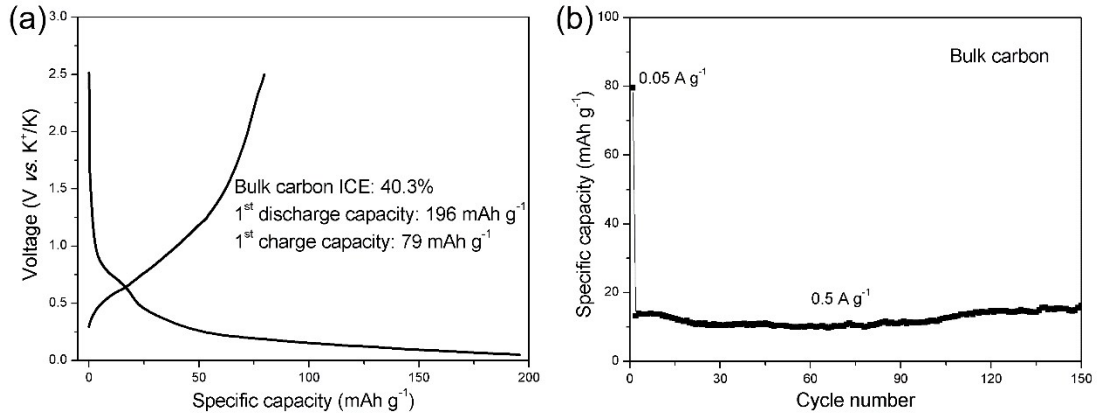

Fig. S5 Electrochemical performance of the alloy-free bulk carbon. (a) Initial discharge/charge curve at 0.05 A g^{-1}. (b) The cycling performance at 0.5 A g^{-1}.

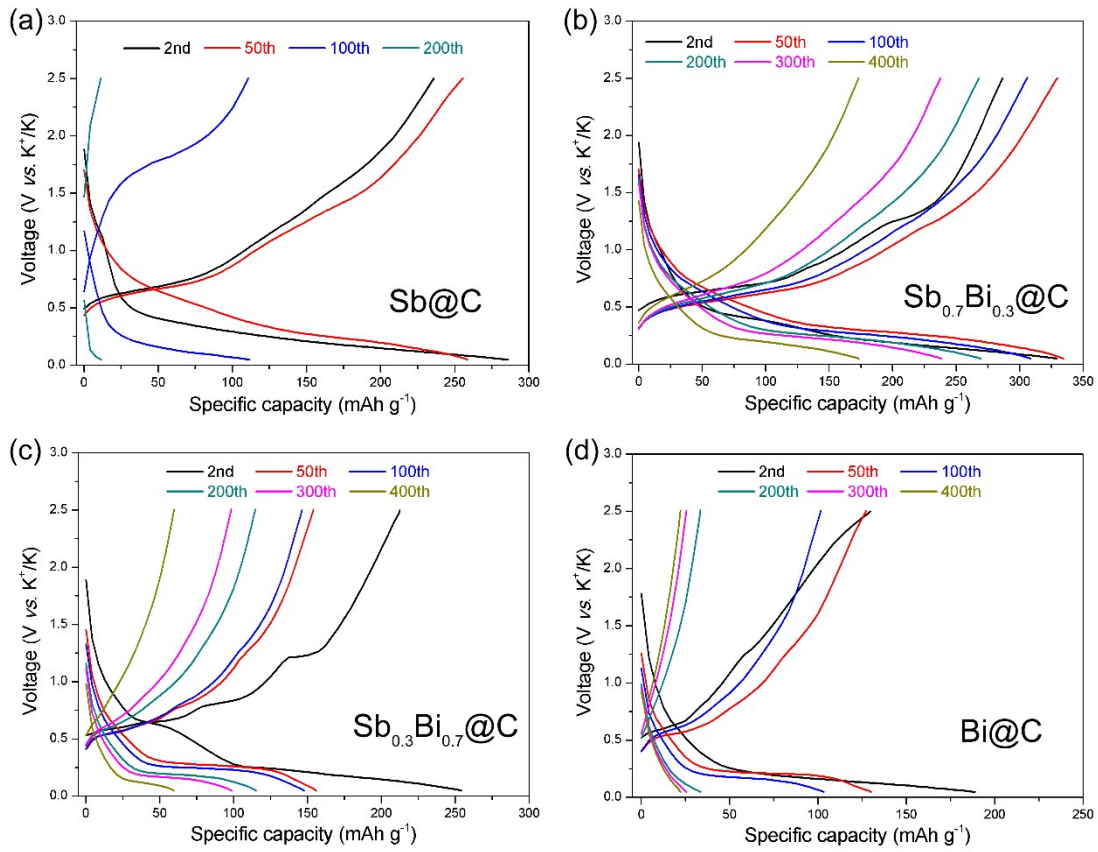

Fig. S6 The discharge/charge curves of (a) Sb@C, (b) $Sb_{0.7}Bi_{0.3}$@C, (c) $Sb_{0.3}Bi_{0.7}$@C and (d) Bi@C in different cycles at 0.5 A g^{-1}.

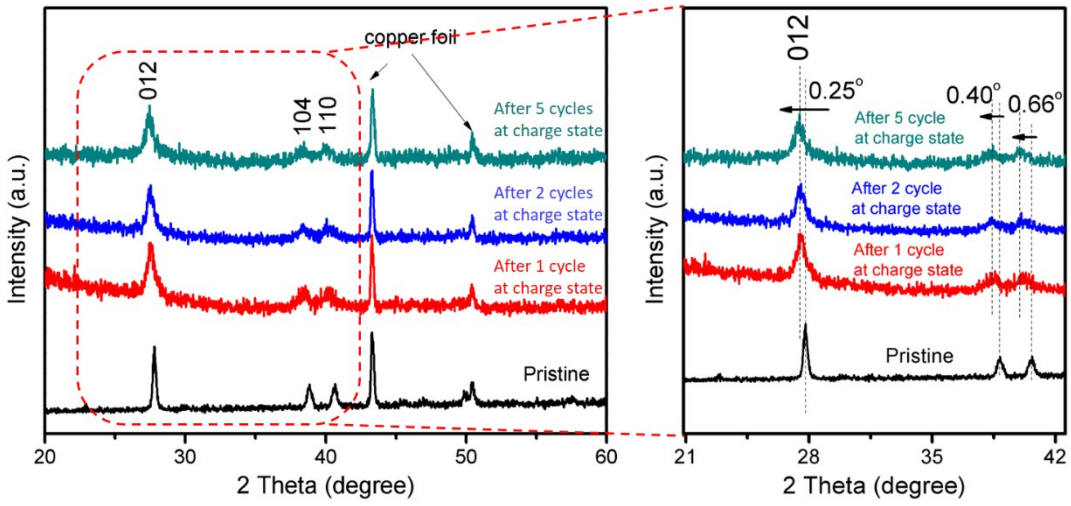

Fig. S7 ex-situ XRD patterns of the $Sb_{0.5}Bi_{0.5}$@C electrode at different cycles.

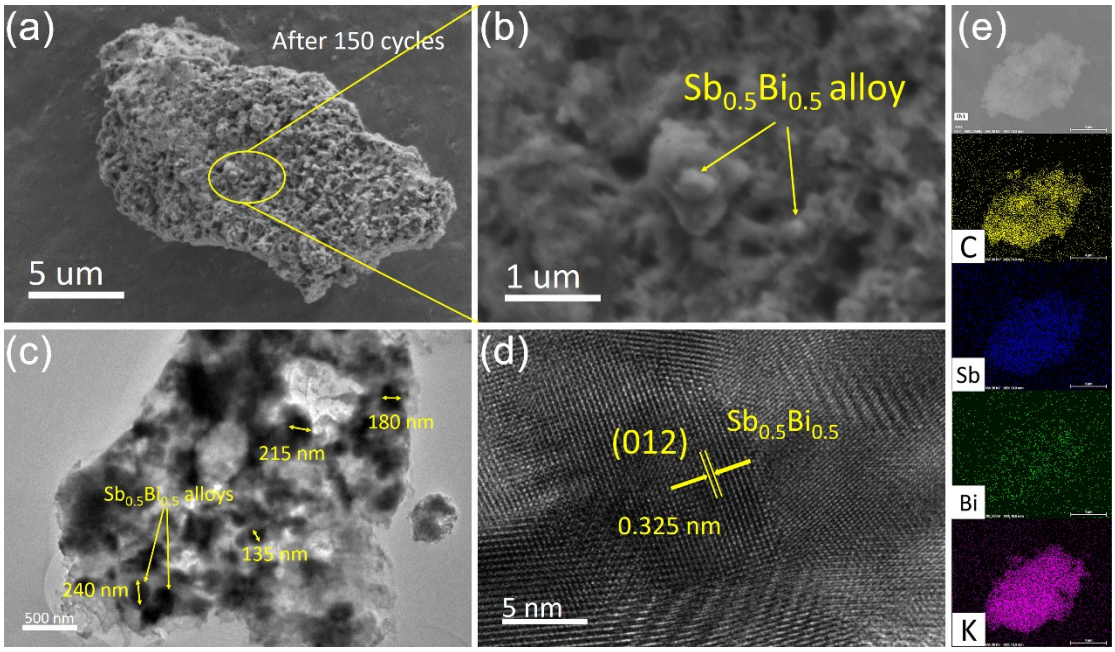

Fig. S8 The morphology characterization of $Sb_{0.5}Bi_{0.5}$@C electrode after 150 cycles. (a, b) SEM. (c, d) TEM and HRTEM. (e) EDS mappings.

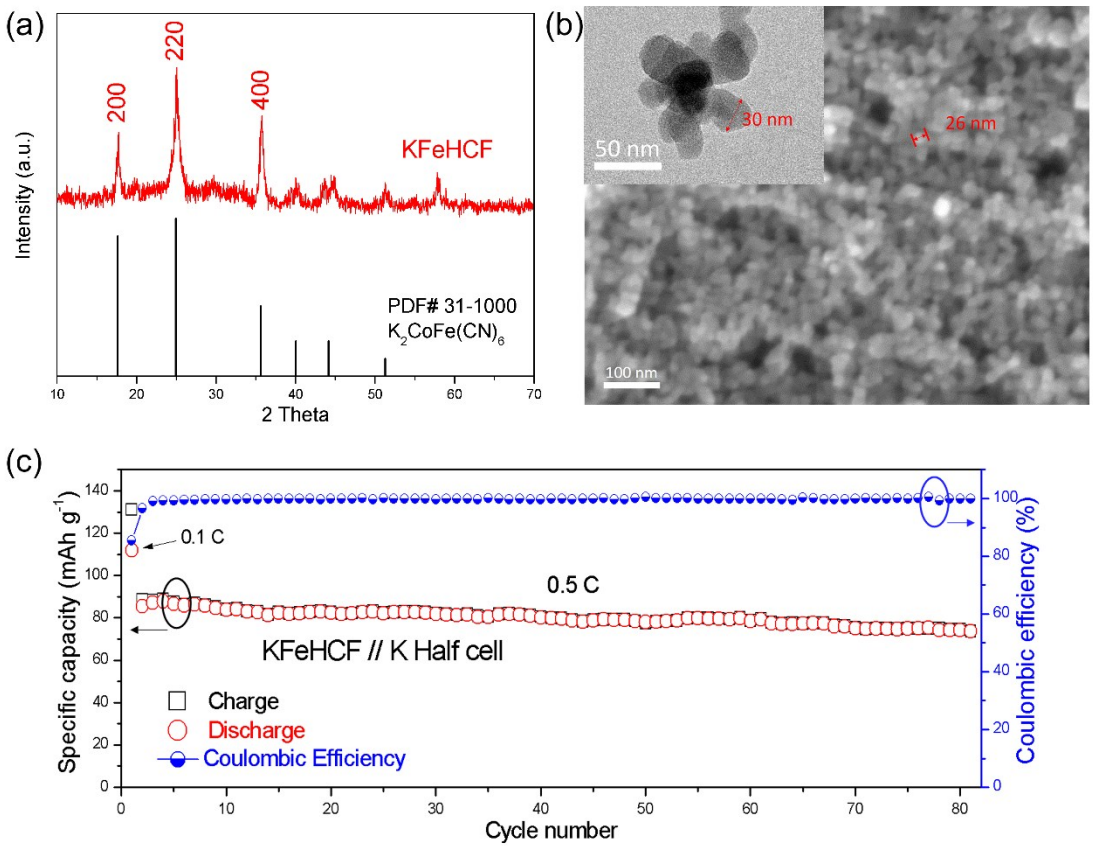

Fig. S9 (a) The XRD pattern of the as synthesized KFeHCF. (b) The FESEM and TEM (inset) images of the KFeHCF. (c) The cycling stability of the KFeHCF//K half-cell at 0.5 C.

Table S1. The comparison of electrochemical properties between this work and previously reported ones.

Anode materials	Reversible capacity (mA h g^{-1})	ICE[a] (%)	Rate capability	Cyclic property	Refs
SnSb	370 at 22 mA g^{-1}	77%	--	76% CR[b] after 40 cycles at 22 mA g^{-1}	1
SnSb@NC	355 at 50 mA g^{-1}	90%	117 mA h g^{-1} at 2 A g^{-1}	80% CR after 200 cycles at 500 mA g^{-1}	2
Sb_2Se_3@C	391 at 100 mA g^{-1}	47%	174 mA h g^{-1} at 2 A g^{-1}	64% CR after 400 cycles at 500 mA g^{-1}	3
$(Bi, Sb)_2S_3$	611 at 100 mA g^{-1}	60%	300 mA h g^{-1} at 1 A g^{-1}	78% CR after 1000 cycles at 500 mA g^{-1}	4
Sb_4P_3@C	540 at 50 mA g^{-1}	64%	170 mA h g^{-1} at 2 A g^{-1}	49% CR after 1000 cycles at 500 mA g^{-1}	5
$Sb_{0.5}Bi_{0.5}$@C	382 at 50 mA g^{-1}	81%	200 mA h g^{-1} at 2 A g^{-1}	83% CR after 400 cycles at 500 mA g^{-1}	This work

[a] The initial Coulombic efficiency (ICE).

[b] Capacity retention (CR)

Table S2. Structural parameters of $Sb_{0.5}Bi_{0.5}$ and $K_3Sb_{0.5}Bi_{0.5}$.

	a	b	c	V_{cell}	Z	V_{cell}/Z
$Sb_{0.5}Bi_{0.5}$	4.432	4.432	11.677	198.6	6	33.1
$K_3Sb_{0.5}Bi_{0.5}$	8.568	8.568	8.568	628.9	4	157.2

The calculation details are demonstrated as following:

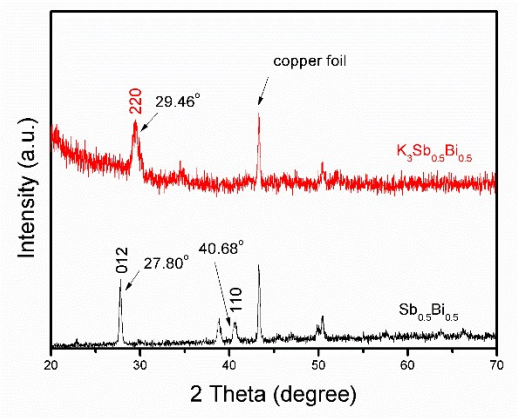

$Sb_{0.5}Bi_{0.5}$ belongs to the space group R-3m. The d-space of it can be illustrated as equation S1:

$$d_{hkl} = \frac{a}{\sqrt{\frac{4}{3}(h^2 + k^2 + hk) + l^2 \frac{a^2}{c^2}}}$$

Equation S1

Meanwhile, it should also meet the Bragg's Law: $2d\sin\theta = n\lambda$ (λ=1.5406)

$$d_{110} = \frac{a}{\sqrt{\frac{4}{3}(1+1+1)+0}} = \frac{a}{2}$$

$$2*d_{110}*\sin(40.68°/2)=1*1.5406$$

Thus, we can calculate that the value of cell parameter a=b=4.432.

$$d_{012} = \frac{a}{\sqrt{\frac{4}{3}(0+1+0)+4\frac{a^2}{c^2}}}$$

$$2*d_{012}*\sin(27.8^o/2)=1*1.5406$$

Thus, we can calculate that the value of cell parameter c=11.677.

$K_3Sb_{0.5}Bi_{0.5}$ belongs to the space group Fm-3m. The d-space of it can be illustrated as equation S2:

$$d_{hkl} = \frac{a}{\sqrt{h^2+k^2+l^2}} \qquad \text{Equation S2}$$

Meanwhile, it should also meet the Bragg's Law: $2d\sin\theta=n\lambda$ (λ=1.5406)

$$d_{220} = \frac{a}{\sqrt{4+4+0}}$$

$$2*d_{220}*\sin(29.46^o/2)=1*1.5406$$

Thus, we can calculate that the value of cell parameter a=b=c=8.568.

The volume expansion from $Sb_{0.5}Bi_{0.5}$ to $K_3Sb_{0.5}Bi_{0.5}$ is (157.2-33.1)/33.1=375%.

Thus the full volume expansion from $Sb_{0.5}Bi_{0.5}$ (a=b=4.432 Å, c=11.677 Å) to $K_3Sb_{0.5}Bi_{0.5}$ (a=b=c=8.568 Å) is calculated to be 375% based on their lattice parameter.

Reference

1 V. Gabaudan, R. Berthelot, M. T. Sougrati, P.-E. Lippens, L. Monconduit, L. Stievano, *J. Mater. Chem. A,* 2019, 7, 15262-15270.

2 Z. Wang, K. Dong, D. Wang, S. Luo, Y. Liu, Q. Wang, Y. Zhang, A. Hao, C. Shi, N. Zhao, *J. Mater. Chem. A,* 2019, 7, 14309-14318.

3 Z. Yi, Y. Qian, J. Tian, K. Shen, N. Lin, Y. Qian, *J. Mater. Chem. A,* 2019, 7, 12283-12291.

4 J. Wang, L. Fan, Z. Liu, S. Chen, Q. Zhang, L. Wang, H. Yang, X. Yu, B. Lu, *ACS Nano,* 2019, 13, 3703-3713.

5 W. Zhang, W. K. Pang, V. Sencadas, Z. Guo, *Joule,* 2018, 2, 1534-1547.